

Analysing Ultra High Energy Cosmic Rays' Anisotropy in $f(R, T)$ Gravity Theory

Swaraj Pratim Sarmah^{*} and Umananda Dev Goswami[†]

Department of Physics, Dibrugarh University, Dibrugarh 786004, Assam, India

In this study, we investigated the anisotropy of diffusive Ultra-High Energy Cosmic Rays (UHECRs) by employing three cosmological models: two models from the $f(R, T)$ gravity theory and the other is the standard Λ CDM model. The primary objective of this work was to ascertain the role of the $f(R, T)$ gravity theory in comprehending the anisotropy of UHECRs without implicitly endorsing the conventional cosmology. We parameterized the magnetic field and the source distance in anisotropy calculations to align well with the observational data from the Pierre Auger Observatory for all the cosmological models. An uncertainty band is presented along with the χ^2 test for all cosmological models to demonstrate the goodness of fitting. Our findings revealed that the amplitude of the anisotropy is highly sensitive to these cosmological models. Notably, the $f(R, T)$ models exhibited a lower amplitude of anisotropy (i.e., more isotropy), while the Λ CDM model predicted a comparatively higher amplitude at most of the energies considered.

PACS numbers: 95.30.Sf, 98.70.Sa, 04.50.Kd

Keywords: Ultra High Energy Cosmic Rays, Anisotropy, $f(R, T)$ gravity

I. INTRODUCTION

It is generally believed that cosmic rays (CRs) with energies below 10^{17} eV are mainly of galactic origin. Though their exact sources remain unknown, they are likely linked to sources such as supernova remnants or pulsars [1–3]. At ultra-high energies (UHEs), above 10^{18} eV, CRs are thought to originate from extragalactic sources [4]. This idea is supported by several observations [5–7]. For instance, their arrival directions show no clear correlation with the distribution of galactic matter [6, 7]. Another key finding is the detection of a dipolar pattern in the arrival directions of CRs with energies above 8 EeV ($1 \text{ EeV} = 10^{18}$ eV), which are pointing away from the galactic centre [8] further supporting their extragalactic origin. The energy spectrum and the arrival directions of CRs are crucial for understanding their nature. Changes in the slope of the spectrum can indicate shifts in propagation processes or transitions between different source populations, such as the dominance of extragalactic sources above the “ankle” around 5 EeV, followed by a softening at approximately 13 EeV [9, 10], and a sharp decline starting near 50 EeV [11, 12]. These shifts may also occur at intermediate energy levels. Furthermore, energy losses due to processes like pair production, as extragalactic protons interact with the cosmic microwave background (CMB) [13–15], or due to diffusion effects [16], can significantly shape the CR spectrum in the EeV energy range.

Significant progress has been made in recent years in the understanding of features of UHECRs. One major finding is a suppression in the CRs flux above 4×10^{19} eV. This suppression has been confirmed by several experiments [9, 17–19]. The decrease in flux at these energies is thought to result from the energy losses during propagation over cosmological distances, a phenomenon predicted nearly fifty years ago, known as the GZK cutoff [20, 21]. However, current data does not conclusively show whether the energy loss is the only factor causing this suppression. Additionally, researchers have set upper limits on the presence of photons [22–24], neutrinos [25–27], and neutrons [28] in UHECRs. Data from the Pierre Auger Observatory (Auger) also indicates that at energies around EeV, CRs are primarily composed of light elements, mainly H and He, but their average mass progressively increases beyond a few EeV [29–34].

As the origins of UHECRs remain unknown, studying the anisotropies in their arrival directions may provide valuable clues in this regard [35–37]. A significant challenge is that UHECRs, being charged particles, are deflected by magnetic fields in both galactic and extragalactic space. As a result, their arrival directions do not directly point to their sources. However, at the highest energies, these deflections become smaller due to the increased momentum of the particles, offering hope for identifying nearby, powerful extragalactic sources. Potential extragalactic sources include gamma-ray bursts, tidal disruption events, active galactic nuclei, and galaxy mergers [5]. The luminosity density of these sources, which depends on their distances (measured by redshift), affects the observed intensity of UHECRs and the production of secondary particles. Interactions with the CMB can cause energy loss, fragmentation of heavier particles, and production of photons and neutrinos through photo-pion interactions. These processes help to explain the UHECR spectrum at the highest energies and the anisotropies observed at intermediate angular scales. The large-scale anisotropies in UHECR arrival directions are linked to the uneven distribution of nearby galaxies within a few hundred Mpc [38]. For energies above 4 EeV, the dipolar anisotropy amplitude increases with energy. Auger has analysed over 2600 UHECR events with energies above 32 EeV, finding a deviation from isotropy at an intermediate angular

* Email: swarajpratimsarmah16@gmail.com

† Email: umananda@dibru.ac.in

scale with a 4σ confidence level [39]. Additionally, Auger data show a 4σ level of disfavoring of isotropy when correlated with starburst galaxies, highlighting their potential role in UHECRs anisotropy [40]. Similar findings have also been reported by the Telescope Array (TA) experiment [41–44]. Alongside the study of arrival direction patterns, understanding how UHECRs’ composition changes with energy is equally important. Lighter and heavier components experience different deflection levels, providing valuable information. The Auger and TA are undergoing upgradation to improve their ability to investigate both anisotropies and composition of CRs at the highest energies.

One of the main challenges in modern cosmology is to explain the late-time cosmic acceleration [45–47]. General relativity (GR), the most robust theory of gravity, struggles to naturally account for the accelerated expansion on cosmological scales, prompting exploration of alternative explanations. These alternatives primarily fall into two categories: dark energy (DE) and modifications or replacement of GR. GR links matter content with spacetime curvature, so any modification must alter one of these two components. DE introduces a form of matter with a repulsive gravitational effect [48]. Many theories of DE have been proposed, yet there is no experimental support for their validity. Almost parallelly, along with the DE the idea of the modification of the geometry part of GR has been developed to tackle the issue of cosmic expansion, leading to the modified theories of gravity (MTGs) [49, 50]. As mentioned, since GR is a geometric theory of gravity, modifying its underlying geometry is a natural approach, forming the basis of modified gravity. A comprehensive review of these theories are provided in Ref. [51]. A straightforward modification of GR replaces the Ricci scalar R in the Einstein-Hilbert (EH) action with a function $f(R)$ of R , resulting in the $f(R)$ gravity theory. Some frameworks based on this approach were discussed in Refs. [52–55]. In passing it needs to be mentioned that the gravity theories that intend to replace GR are based on different geometries of spacetime than one based on GR. These theories are usually termed as alternative theories of gravity (ATGs). One of the recently most focused ATGs is the $f(Q)$ gravity theory [56–61], which is based on the modified symmetric teleparallelism [62, 63].

Another promising approach of MTGs involves coupling geometry with matter. Non-minimal couplings (NMCs) [64] address issues like post-inflationary preheating [65] and large-scale structure formation [66]. Scalar-tensor theories of gravity [67, 68] are based on the idea of MMC. Specifically, the $f(R, L_m)$ gravity [69] incorporates the matter Lagrangian L_m into the action, while $f(R, T)$ gravity [70] generalises it further by including the trace T of the energy-momentum tensor (EMT). The field equations in $f(R, T)$ gravity depend on a source term involving EMT variation, introducing coupling-induced acceleration and non-geodesic particle motion. Similar to some of the viable MTGs, the studies with $f(R, T)$ gravity span diverse areas like thermodynamics [71], scalar perturbations [72] and dark matter implications [73] of the Universe. Other studies with this gravity theory address the cosmic coincidence [74] and gravitational waves [75, 76], showcasing its versatility in modeling cosmological phenomena.

Till now various research groups have employed diverse methods to investigate the anisotropy and propagation of CRs [4, 5, 34, 77–84]. In our previous works, we have explored the flux characteristics [85] and anisotropic properties [86] of UHECRs for a single source within the framework of $f(R)$ gravity. Additionally, we have examined their propagation [87] and flux suppression [88] in this modified gravity theory along with the $f(Q)$ gravity theory for multiple sources. Building on these motivations, the current study aims to extend the investigation of CR anisotropies using an ensemble of sources, especially within the realm of $f(R, T)$ gravity, for the first time. For this purpose, we consider two models of $f(R, T)$ gravity, comparing their predictions with those of the standard Λ CDM model. To validate our results from the observational point of view, we utilize the surface detectors’ data of Auger [89]. The primary goal of this work is to assess the impact of $f(R, T)$ gravity on the anisotropic behaviour of UHECRs in comparison with predictions from standard cosmological models and constraining with observational data.

The rest of this paper is organized as follows. Section II is dedicated to the theoretical formalisms of the diffusion of UHECRs in turbulent magnetic fields (TMFs). Since this study considers the $f(R, T)$ gravity theory as the fundamental cosmological framework for investigating the anisotropy of UHECRs in galactic and extragalactic spaces, in Section III, we present the required cosmological equations in this gravity theory. Section IV briefly discusses the $f(R, T)$ gravity models employed in this study. For an ensemble of sources, the CR anisotropy is analyzed in Section V. The numerical calculations of UHECRs anisotropies for the considered models, along with their comparison to observational data, are discussed in Section VI. Finally, we summarize our results and provide concluding remarks in Section VII.

II. TURBULENT MAGNETIC FIELDS AND DIFFUSION OF COSMIC RAYS

Due to some difficulties, it is hard to model the extragalactic magnetic fields [90]. Their exact strengths are uncertain and they vary across different regions of extragalactic space [91, 92]. At the centres of galaxy clusters, the field strength of these magnetic fields ranges from a few to tens of μG [90]. In less dense areas, they are weaker, typically between 1 and 10 nG, suggesting the presence of larger magnetic fields along cosmic structures like filaments. The coherence length l_c is the maximum distance over which magnetic fields remain correlated. Galactic magnetic fields (GMF), with strengths of a few μG , have minimal impact on the CR spectrum due to their limited size, though they can influence the arrival directions of CRs. To simplify our study, we focus on the propagation of CRs in a turbulent and uniform extragalactic magnetic field. The key properties of this field are its root mean square (RMS) strength B and coherence length l_c . Here, B is defined as $\sqrt{\langle B^2(x) \rangle}$ and typically ranges from 1 nG

to 100 nG [93–95], while l_c varies from 0.01 Mpc to 1 Mpc [96].

The effective Larmor radius of a charged particle with charge Ze and energy E in a magnetic field of strength B is given by

$$r_L = \frac{E}{ZeB} \simeq 1.1 \frac{E/\text{EeV}}{ZB/\text{nG}} \text{ Mpc}. \quad (1)$$

A critical concept in charged particle diffusion is the critical energy E_c . It is defined as the energy at which the particle's Larmor radius equals the coherence length, i.e. $r_L(E_c) = l_c$. The critical energy is expressed as

$$E_c = ZeBl_c \simeq 0.9Z \frac{B}{\text{nG}} \frac{l_c}{\text{Mpc}} \text{ EeV}. \quad (2)$$

In Ref. [4], using a numerical simulation the diffusion coefficient D as a function of energy is provided as

$$D(E) \simeq \frac{cl_c}{3} \left[4 \left(\frac{E}{E_c} \right)^2 + a_I \left(\frac{E}{E_c} \right) + a_L \left(\frac{E}{E_c} \right)^{2-\gamma} \right], \quad (3)$$

where γ is the spectral index, and a_I and a_L are two coefficients. For a Kolmogorov spectrum [34] in a TMF, $\gamma = 5/3$ with $a_L \simeq 0.23$ and $a_I \simeq 0.9$. The diffusion length l_D , representing the distance at which a particle's deflection is about one radian is defined as $l_D = 3D/c$. Using Eq. (3), for $E/E_c \ll 0.1$, the diffusion length can be approximated as $l_D \simeq a_L l_c (E/E_c)^{2-\delta}$ and for $E/E_c \gg 0.2$, it is $l_D \simeq 4l_c (E/E_c)^2$ [34].

In the diffusive regime, the transport equation for UHE particles is given as [97]

$$\frac{\partial n}{\partial t} + 3H(t)n - b(E, t) \frac{\partial n}{\partial E} - \frac{D(E, t)}{a^2(t)} \nabla^2 n = \frac{\mathcal{N}(E, t)}{a^3(t)} \delta^3(x - \mathbf{x}_s), \quad (4)$$

where $H(t) = \dot{a}(t)/a(t)$ is the Hubble parameter, $\dot{a}(t)$ is the time derivative of the scale factor $a(t)$, x is the comoving coordinate and $r_s = (x - \mathbf{x}_s)$ is the source distance. n is the particle density and $\mathcal{N}(E)$ describes the number of particles emitted with energy E per unit time. The energy losses (adiabatic and interaction losses), caused by cosmic expansion and interactions with the CMB are given by [4]

$$\frac{dE}{dt} = -b(E, t), \quad b(E, t) = H(t)E + b_{\text{int}}(E). \quad (5)$$

Here b_{int} denotes the energy losses due to interaction with CMB and it includes both photopion and pair production. The general solution of Eq. (4) is [97]

$$n(E, r_s) = \int_0^{z_i} dz \left| \frac{dt}{dz} \right| \mathcal{N}(E_g, z) \frac{\exp[-r_s^2/4\lambda^2]}{(4\pi\lambda^2)^{3/2}} \frac{dE_g}{dE}, \quad (6)$$

where $E_g(E, z)$ represents the generation energy at redshift z and \mathcal{N} represents the source emissivity. The Syrovatskii variable λ^2 [98] is defined as

$$\lambda^2(E, z) = \int_0^z dz \left| \frac{dt}{dz} \right| (1+z)^2 D(E_g, z). \quad (7)$$

Here $D(E_g, z)$ is the diffusion coefficient for the generation energy at z . In the diffusive regime, the particle density increases with energy, distance from the source and TMF properties. This density enhancement describes how the CRs density evolves during propagation through intergalactic space and interactions with the CMB [85]. It is quantified as the ratio of the density obtained from rectilinear propagation to actual density [34]:

$$\xi(E, r_s) = \frac{4\pi r_s^2 c n(E, r_s)}{\mathcal{N}(E)}. \quad (8)$$

For multiple sources, the source distance r_s is replaced by r_i , which is discussed further in Section V.

III. BASIC EQUATIONS OF $f(R, T)$ GRAVITY

The total action of the $f(R, T)$ gravity is given by [70]

$$S = \frac{1}{2\kappa} \int f(R, T) \sqrt{-g} d^4x + \int \mathcal{L}_m \sqrt{-g} d^4x, \quad (9)$$

where $\kappa = 8\pi$, R is the Ricci scalar, T is the trace of of the energy-momentum tensor $T_{\mu\nu}$, g is the determinant of the metric tensor $g_{\mu\nu}$ and \mathcal{L}_m is the matter Lagrangian. As discussed earlier, $f(R, T)$ is a function of both R and T . Here we used the geometrized unit system wherein $G = c = 1$. Varying the action (9) with respect to the metric tensor $g_{\mu\nu}$ yields the field equations of $f(R, T)$ gravity as given by [70]

$$f_R(R, T)R_{\mu\nu} - \frac{1}{2}f(R, T)g_{\mu\nu} + (g_{\mu\nu}\square - \nabla_\mu\nabla_\nu)f(R, T) = \kappa T_{\mu\nu} - f_T(R, T)T_{\mu\nu} - f_T(R, T)\Theta_{\mu\nu}, \quad (10)$$

where $f_R = \partial f/\partial R$, $f_T = \partial f/\partial T$, ∇_μ is the covariant derivative and $\square = \nabla^\mu\nabla_\mu$ is the d'Alembertian operator. The tensor $\Theta_{\mu\nu}$ depends on the matter Lagrangian and simplifies for a perfect fluid as [70]

$$\Theta_{\mu\nu} = -2T_{\mu\nu} + pg_{\mu\nu}. \quad (11)$$

and the energy-momentum tensor is defined as

$$T_{\mu\nu} = -\frac{2}{\sqrt{-g}}\frac{\delta(\sqrt{-g}\mathcal{L}_m)}{\delta g^{\mu\nu}}, \quad (12)$$

with its trace $T = g^{\mu\nu}T_{\mu\nu}$. In a spatially flat Friedmann-Lemaître-Robertson-Walker (FLRW) spacetime with metric

$$ds^2 = -dt^2 + a^2(t)(dx^2 + dy^2 + dz^2), \quad (13)$$

the modified Friedmann equations are

$$3H^2 f_R + \frac{1}{2}(f - Rf_R) + 3H\dot{f}_R = (\kappa + f_T)\rho, \quad (14)$$

$$2\dot{H}f_R + \ddot{f}_R - H\dot{f}_R = -(\kappa + f_T)\rho, \quad (15)$$

where $H = \dot{a}/a$ is the Hubble parameter as mentioned earlier, ρ and p are the total energy density and pressure of the Universe. These two equations can be expressed as effective Friedmann equations as follows [99]:

$$3H^2 = \kappa\rho_{\text{eff}} = \kappa(\rho + \rho_{\text{mod}}), \quad (16)$$

$$2\dot{H} + 3H^2 = -\kappa(\rho_{\text{eff}} + p_{\text{eff}}), \quad (17)$$

where $\rho_{\text{eff}} = \rho + \rho_{\text{mod}}$ and $p_{\text{eff}} = p + p_{\text{mod}}$ (for pressure less dust $p = 0$) with ρ_{mod} and p_{mod} are contributions to the energy density and pressure of the Universe from the modified gravity, effectively behaving like a dark fluid component as given by [99]

$$\rho_{\text{mod}} = \frac{-f(R, T) - 6H\dot{f}_R + 2(\kappa + f_T)\rho + f_R(R - 2\kappa\rho)}{2\kappa f_R} \quad (18)$$

and

$$p_{\text{eff}} = p_{\text{mod}} = \frac{3\left[\ddot{f}_R + f(R, T) + 5H\dot{f}_R - Rf_R - (f_T + \kappa)\rho\right]}{3\kappa f_R}. \quad (19)$$

Generally, the trace of the energy-momentum tensor for a perfect fluid is given by $T = \rho + 3p$. However, we can rewrite this expression for the pressure-less dust as $T = \sigma\rho$, where σ is a parameter of adjustment.

IV. $f(R, T)$ GRAVITY MODELS

This section outlines the $f(R, T)$ gravity cosmological models used to compute the cosmological parameters required for this study. In particular, we consider two models of $f(R, T)$ gravity that include both minimal and non-minimal coupling between curvature and matter. Also, the expression for the Hubble parameter $H(z)$ for these models is presented in this section.

A. Model I: Minimal coupling in exponential form

The first $f(R, T)$ gravity model we have considered here is given by [99]

$$f(R, T) = \alpha R + \beta e^T, \quad (20)$$

where α and β are two model parameters. For this model the first Friedmann Eq. (16) takes the form [99]:

$$H^2(z) = \frac{1}{6\alpha} \left[2(\rho_{m0} + \rho_{rad0}(1+z))(1+z)^3 + \beta \left(2\rho_{m0}(1+z)^3 - 1 \right) e^{\sigma\rho_{m0}(1+z)^3} \right], \quad (21)$$

where ρ_{m0} and ρ_{rad0} are matter and radiation components of the energy density ρ of the Universe. The respective dimensionless density parameters are defined as

$$\Omega_{m0} = \frac{\rho_{m0}}{3H_0^2}, \quad \Omega_{rad0} = \frac{\rho_{rad0}}{3H_0^2}. \quad (22)$$

Using these dimensionless density parameters Eq. (21) can be rewritten as

$$H(z) = \frac{H_0}{\sqrt{2\alpha}} \left[2(\Omega_{m0} + \Omega_{rad0}(1+z))(1+z)^3 + \beta \left(2\Omega_{m0}(1+z)^3 - (3H_0^2)^{-1} \right) e^{3H_0^2\sigma\Omega_{m0}(1+z)^3} \right]^{1/2}. \quad (23)$$

In this work we used the values of the model parameters as $\alpha = 0.8469$, $\beta = -0.4285$, and $\sigma = -0.0041$. These parameter values represent the best-fit results obtained using cosmic chronometer (CC) and Baryon Acoustic Oscillation (BAO) data [99].

B. Model II: Non-minimal coupling

The second model we have considered is a model of non-minimal coupling between matter and gravity, and is given by [99]

$$f(R, T) = R + f_0 R T^\delta, \quad (24)$$

where $f_0 \neq 0$ and δ are parameters of this model. For this model, the first Friedmann Eq. (16) can be expressed as [99]

$$H^2(z) = \frac{\left[\sigma(\rho_{m0} + \rho_{rad0}(1+z)) + f_0(\sigma\rho_{m0}(1+z)^3)^\delta (\sigma\rho_{m0} + \rho_{rad0}(\sigma - \delta)(1+z)) \right]}{\sigma + f_0(3\delta + \sigma)(\sigma\rho_{m0}(1+z)^3)^\delta} \times (1+z)^3 \left[\frac{4\sigma}{3 \left\{ \sigma + f_0(\sigma - \delta)(\sigma\rho_{m0}(1+z)^3)^\delta \right\}} - \frac{1}{1 + f_0(\sigma\rho_{m0}(1+z)^3)^\delta} \right]. \quad (25)$$

By using the dimensionless density parameters from Eq. (22), we can write the above equation in the form:

$$H(z) = H_0 \frac{\left[3\sigma(\Omega_{m0} + \Omega_{rad0}(1+z)) + 3f_0(H_0^2)^\delta (3\sigma\Omega_{m0}(1+z)^3)^\delta (\sigma\Omega_{m0} + \Omega_{rad0}(\sigma - \delta)(1+z)) \right]^{1/2}}{\left[\sigma + f_0(3\delta + \sigma)(3H_0^2\sigma\Omega_{m0}(1+z)^3)^\delta \right]^{1/2}} \times (1+z)^{3/2} \left[\frac{4\sigma}{3 \left\{ \sigma + f_0(\sigma - \delta)(3H_0^2\sigma\Omega_{m0}(1+z)^3)^\delta \right\}} - \frac{1}{1 + f_0(3H_0^2\sigma\Omega_{m0}(1+z)^3)^\delta} \right]^{1/2}. \quad (26)$$

The values of the model parameters we have used for this study are $f_0 = 2.4285$, $\sigma = 0.1836$ and $\delta = 0.1002$ [99]. Some other cosmological parameters that we have used in this work are $H_0 \approx 67.4 \text{ km s}^{-1} \text{ Mpc}^{-1}$ [100], $\Omega_{m0} \approx 0.315$ [100], and

$\Omega_{r0} \approx 5.373 \times 10^{-5}$ [101]. The cosmological time evolution with respect to redshift that appears in Eq. (6) can be expressed as [85]

$$\left| \frac{dt}{dz} \right| = \frac{1}{(1+z)H}. \quad (27)$$

Using this equation with the expressions of the Hubble parameter for the model considered above, the cosmological time evolution with respect to redshift for the corresponding cosmological models can be calculated.

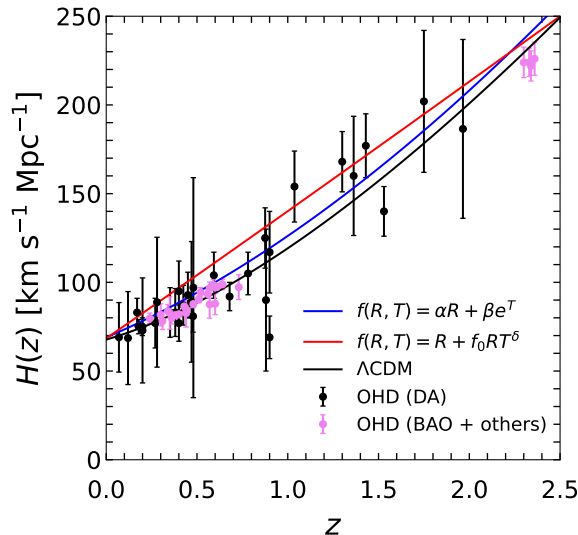


FIG. 1. Variations of Hubble parameter $H(z)$ with redshift z as predicted by the $f(R, T)$ gravity models along with the Λ CDM model, and in comparison with the observational Hubble data (OHD) obtained from Differential Age (DA) and BAO methods [85, 102].

We compare the Hubble parameter results obtained for both $f(R, T)$ gravity models, and the standard Λ CDM model along with the observational Hubble data (OHD) acquired from Differential Age (DA) and BAO methods [85, 102] in Fig. 1. The plot demonstrates that both $f(R, T)$ gravity models' results fit well with the observational data.

V. ANISOTROPY OF COSMIC RAYS FOR AN ENSEMBLE OF SOURCES

The flux from a CR source at a distance r_s , much greater than the diffusion length l_D can be calculated by solving the diffusion equation in the expanding Universe [97]. The resulting expression is given as [103]

$$J(E) = \frac{c}{4\pi} \int_0^{z_{\max}} dz \left| \frac{dt}{dz} \right| \mathcal{N}[E_g(E, z), z] \frac{\exp[-r_s^2/(4\lambda^2)]}{(4\pi\lambda^2)^{3/2}} \frac{dE_g}{dE}, \quad (28)$$

where z_{\max} is the maximum redshift at which the CRs emitting by a source can be perceived. Since we focus on multiple sources rather than a single source, we employ a relation given by [103, 104],

$$r_i = \left(\frac{3}{4\pi} \right)^{1/3} d_s \frac{\Gamma(i+1/3)}{(i-1)!}, \quad (29)$$

where d_s represents the distance between the sources and i indicates the i -th source from the average distance. The term d_s is linked with the source density n_s as $d_s \approx n_s^{-1/3}$. Consequently, for a discrete source distribution, summing over the sources results in a specific factor [103, 104]:

$$F \equiv \frac{1}{n_s} \sum_i \frac{\exp[-r_i^2/4\lambda^2]}{(4\pi\lambda^2)^{3/2}}. \quad (30)$$

Subsequently, in Eq. (28), after summing all the sources, we can express the modified flux for an ensemble of sources in terms of the Hubble radius $R_H = c/H_0$ for the first $f(R, T)$ gravity model as

$$J(E)\Big|_{\text{mod-1}} \simeq \frac{R_H n_s}{4\pi} \int_0^{z_{\text{max}}} dz (1+z)^{-1} \times \left[\frac{1}{\sqrt{2\alpha}} \left\{ 2(\Omega_{m0} + \Omega_{rad0}(1+z))(1+z)^3 \right. \right. \\ \left. \left. + \beta \left(2\Omega_{m0}(1+z)^3 - (3H_0^2)^{-1} \right) e^{3H_0^2\sigma\Omega_{m0}(1+z)^3} \right\}^{1/2} \right] \mathcal{N}[E_g(E, z), z] \frac{dE_g}{dE} F. \quad (31)$$

Similarly, for the second $f(R, T)$ gravity model, the modified flux can be expressed as follows:

$$J(E)\Big|_{\text{mod-2}} \simeq \frac{R_H n_s}{4\pi} \int_0^{z_{\text{max}}} dz (1+z)^{-1} \times \\ \left[\frac{\left\{ 3\sigma(\Omega_{m0} + \Omega_{rad0}(1+z)) + 3f_0(H_0^2)^\delta (3\sigma\Omega_{m0}(1+z)^3)^\delta (\sigma\Omega_{m0} + \Omega_{rad0}(\sigma - \delta)(1+z)) \right\}^{1/2}}{\left[\sigma + f_0(3\delta + \sigma)(3H_0^2\sigma\Omega_{m0}(1+z)^3)^\delta \right]^{1/2}} \times \\ (1+z)^{3/2} \left[\frac{4\sigma}{3 \left\{ \sigma + f_0(\sigma - \delta)(3H_0^2\sigma\Omega_{m0}(1+z)^3)^\delta \right\}} - \frac{1}{1 + f_0(3H_0^2\sigma\Omega_{m0}(1+z)^3)^\delta} \right]^{1/2} \right] \times \\ \mathcal{N}[E_g(E, z), z] \frac{dE_g}{dE} F. \quad (32)$$

Furthermore, we can rewrite Eq. (7) in terms of the Hubble radius R_H and using Eq. (3) as

$$\lambda^2(E, z) = H_0 \frac{R_H l_c}{3} \int_0^z dz \left| \frac{dt}{dz} \right| (1+z)^2 \left[4 \left(\frac{(1+z)E}{E_c} \right)^2 + a_I \left(\frac{(1+z)E}{E_c} \right) + a_L \left(\frac{(1+z)E}{E_c} \right)^{2-\gamma} \right]. \quad (33)$$

Now we calculate the density enhancement factor of CR protons for the $f(R, T)$ gravity models. Using this result, we compute the CR protons' flux and ultimately their anisotropy as predicted by the two $f(R, T)$ gravity models. The anisotropy is evaluated following the methodology outlined in Ref. [105] and which is expressed as

$$\Delta = 3 \frac{\eta}{\xi}, \quad (34)$$

where η is the modification factor as given by (see Refs. [85, 86])

$$\eta = \frac{J(E)}{J_0(E)}. \quad (35)$$

Here, $J_0(E)$ is the CR flux without any kind of energy losses and it is given by

$$J_0(E) = \frac{c}{4\pi} \int_0^{z_{\text{max}}} dz \left| \frac{dt}{dz} \right| \mathcal{N}_{z \rightarrow 0}(E) \frac{\exp[-r_s^2/(4\lambda^2)]}{(4\pi\lambda^2)^{3/2}}. \quad (36)$$

Utilizing these aforementioned relations within the framework of the contemplated models of MTGs, we will analyse the numerical outcomes pertaining to the anisotropy in the ensuing section.

VI. RESULTS AND DISCUSSION

This section focuses on numerical computations, data fitting, and analysis of results. The `python` `scipy` and `numpy` libraries are used for the numerical calculations, while `matplotlib` is used for creating plots. All the plots presented assume the primary particles as protons with a spectral index $\gamma = 2$ and the redshift $z = 2$.

Fig. 2 presents the UHECRs anisotropy parameter Δ as a function of energy E (in EeV) for different theoretical models, compared with the Auger SD 750 (blue points) and SD 1500 (red points) datasets. The magenta and green lines represent the first and second $f(R, T)$ gravity models respectively, and the black line corresponds to the standard Λ CDM model. For this plot

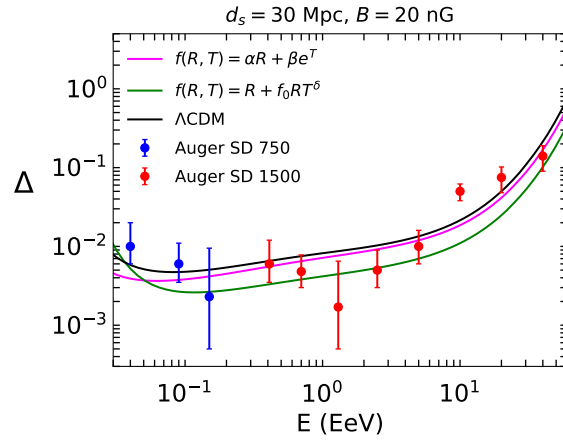


FIG. 2. The anisotropy of UHECRs as a function of energy E for two $f(R, T)$ gravity models along with the standard Λ CDM model for $d_s = 30$ Mpc and $B = 20$ nG. The observational data are taken from the Auger [89].

the values of the magnetic field (B) and source separation distance (d_s) are fixed at 20 nG and 30 Mpc respectively, for all cases. The anisotropy prediction of the Λ CDM model shows a steady increase from $\Delta \sim 4 \times 10^{-3}$ at low energies (< 0.1 EeV) to higher values beyond 10 EeV. The experimental data align reasonably well with the curve at low energies. The $f(R, T) = \alpha R + \beta e^T$ model predicts a similar qualitative trend but shows a slight suppression of anisotropy at low energies compared to the Λ CDM. The $f(R, T) = R + f_0 RT^\delta$ model also exhibits anisotropy suppression compared to Λ CDM at intermediate (> 0.1 EeV) and high energies (> 10 EeV). At low energies, all three models provide a similar trend of predictions, which align well with the experimental data. At intermediate and high energies, the $f(R, T)$ gravity models deviate from the Λ CDM prediction, potentially reflecting modified gravity effects. However, significant scatter in the high energy experimental data and deviations from theoretical trends suggest the need for further refinements in both observational and theoretical approaches. We will take the fitting parameters of the Λ CDM model as reference and based on them, modify those parameters for the $f(R, T)$ gravity model.

Fig. 3 shows the updated theoretical predictions for the two $f(R, T)$ gravity models, where adjustments in the magnetic field (B) and source separation distance (d_s) are performed to improve alignment with the Auger SD 750 and SD 1500 datasets. In the left panel, corresponding to the model $f(R, T) = \alpha R + \beta e^T$, the parameters are set to $d_s = 30$ Mpc and $B = 65$ nG. The theoretical curve maintains a similar qualitative trend to the previous figure but exhibits a slightly better match with the experimental data, particularly at low and intermediate energies. In the right panel, for the model $f(R, T) = R + f_0 RT^\delta$,

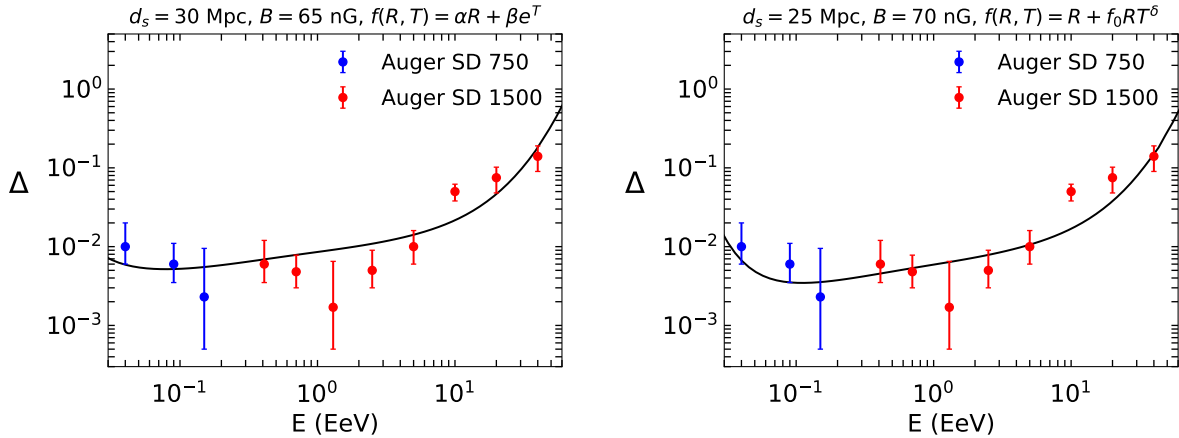


FIG. 3. Left: The modified anisotropy of UHECRs as a function of energy E for the $f(R, T) = \alpha R + \beta e^T$ model with $d_s = 30$ Mpc and $B = 65$ nG. Right: The modified anisotropy of the UHECRs as a function of energy E for the $f(R, T) = R + f_0 RT^\delta$ model with $d_s = 25$ Mpc and $B = 70$ nG. The observational data are taken from the Auger [89].

the parameters are adjusted to $d_s = 25$ Mpc and $B = 70$ nG. The resulting theoretical curve aligns more closely with the Auger SD 750 and SD 1500 data compared to the previous figure, especially at low energies. While in the high energy rise in anisotropy remains a common feature of both models, the adjustments lead to reduced discrepancies with the experimental data.

The chi-squared (χ^2) values for models' predictions are calculated using the formula:

$$\chi^2 = \sum \left(\frac{O_i - M_i}{\sigma_i} \right)^2, \quad (37)$$

where O_i is the i th observed value, M_i is the corresponding model-predicted value, σ_i is the uncertainty in the observation. For the first model, the total χ^2 value is 20.591, for the second model it is 18.276, and for the Λ CDM model it is 16.552. The corresponding reduced χ^2 values are 0.981, 0.870, and 0.788, respectively.

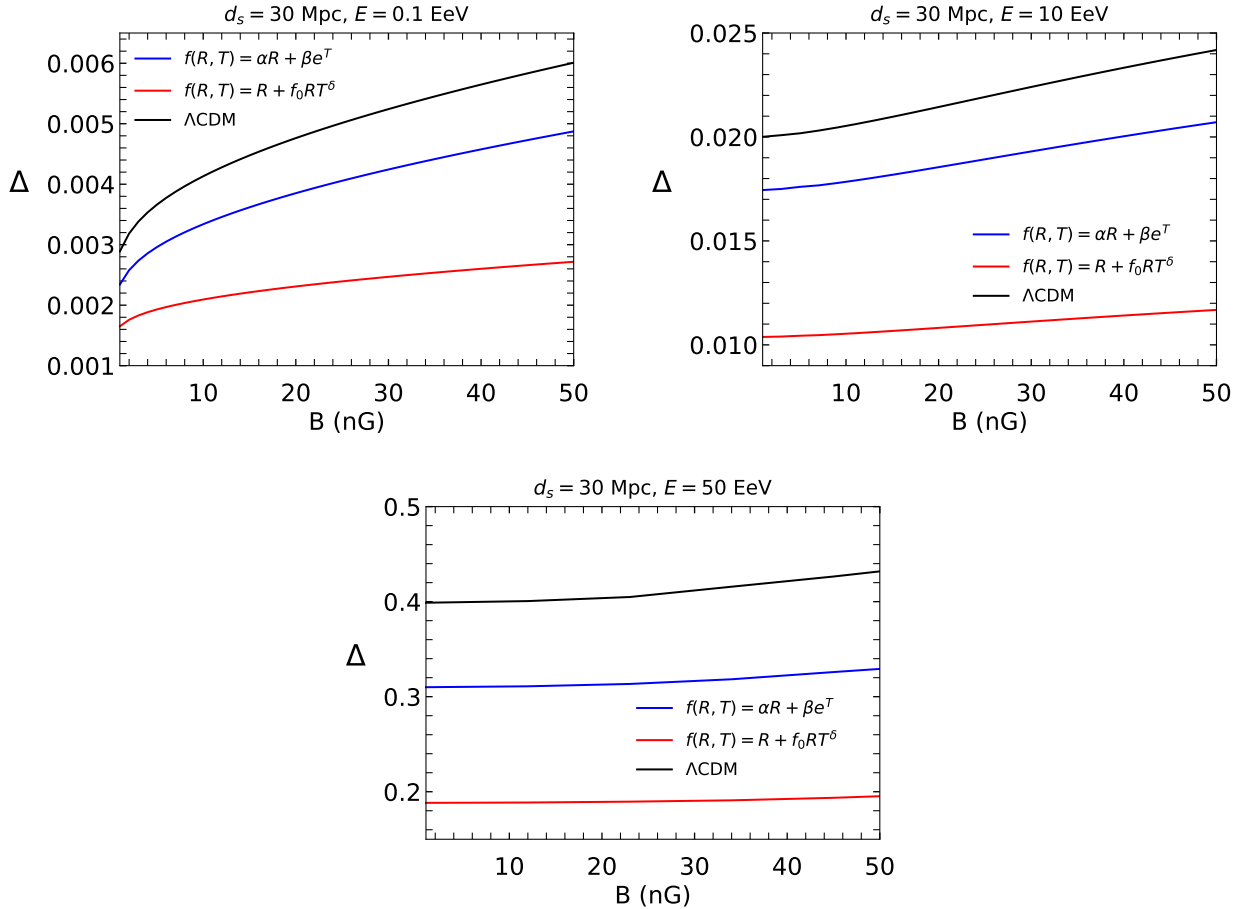


FIG. 4. The anisotropy of the UHECRs as a function of the magnetic field B for two $f(R, T)$ gravity models along with the standard Λ CDM model with $d_s = 30$ Mpc and $E = 0.1$ EeV (left), 10 EeV (right), and 50 EeV (bottom).

Fig. 4 depicts the variation of the anisotropy parameter Δ as a function of the magnetic field strength B (in nG) for three specific CR energies $E = 0.1$ EeV, $E = 10$ EeV, and $E = 50$ EeV in the left, right and bottom panels respectively. The three curves in each plot correspond to different cosmological models: Λ CDM (black), $f(R, T) = \alpha R + \beta e^T$ (blue) and $f(R, T) = R + f_0 R T^\delta$ (red). Across all models and energies, Δ increases with B , reflecting the impact of stronger magnetic fields on CRs' deflection. For a fixed B , the anisotropy parameter Δ increases with energy, as higher energy CRs experience reduced deflection and retain more directional information as it shows a flattened pattern. Among the models, Λ CDM predicts the largest anisotropy for all energies, followed by the $f(R, T) = \alpha R + \beta e^T$ model, while the $f(R, T) = R + f_0 R T^\delta$ model exhibits the lowest values of Δ . This indicates that the underlying cosmological model influences the predicted anisotropy, with MTG models generally predicting smaller anisotropy compared to the standard Λ CDM framework.

These parameter adjustments highlight the sensitivity of anisotropy predictions to different factors such as the magnetic field and source separation distance. The improved alignment of the theoretical predictions with the data underscores the potential of modified gravity models to explain CRs' anisotropy while demonstrating the need for precise tuning of model parameters.

VII. CONCLUSION

In this work, we have studied the CRs' anisotropy parameter Δ as a function of energy E in the UHE range in the framework of two $f(R, T)$ gravity models in comparison to the standard Λ CDM model. To account for the effects of different parameters on the anisotropy, we have explored various magnetic field strengths (B) and source distance separations (d_s). The comparison of the CRs' anisotropy parameter Δ across different theoretical models (Λ CDM and two $f(R, T)$ gravity models) highlights the potential of modified gravity theories to affect in the CRs study. The adjustments to the magnetic field strength (B) and source separation distance (d_s) in the $f(R, T)$ models have demonstrated significant improvements in aligning theoretical predictions with the Auger SD 750 and SD 1500 datasets.

The Λ CDM model provides a reasonable qualitative description of the anisotropy trends at both lower and higher energies with the observed data. In contrast, in the same range of magnetic field and source separation, the $f(R, T) = \alpha R + \beta e^T$ model captures the of anisotropy at higher energies more effectively but does not fit well in the low energies. The $f(R, T) = R + f_0 R T^\delta$ model further refines the alignment at low energies but depicts a deviation at high and intermediate energy with observational trends. Thus, the magnetic field and separation distance modification is required for the $f(R, T)$ models, which is shown in Fig. 3, and now both models are fitted well in both low and high energy regimes. The corresponding χ^2 values depict these all. The analysis of the anisotropy parameter Δ as a function of the magnetic field strength B for different CR energies in Fig. 4 highlights the influence of both magnetic and gravitational effects on CRs propagation. The results demonstrate that MTG models, such as $f(R, T) = \alpha R + \beta e^T$ and $f(R, T) = R + f_0 R T^\delta$, predict lower anisotropy compared to the standard Λ CDM model. These findings emphasize the sensitivity of anisotropy to underlying gravitational frameworks and various factors like the magnetic field, offering a potential avenue to distinguish between standard and MTGs through observations of UHECRs.

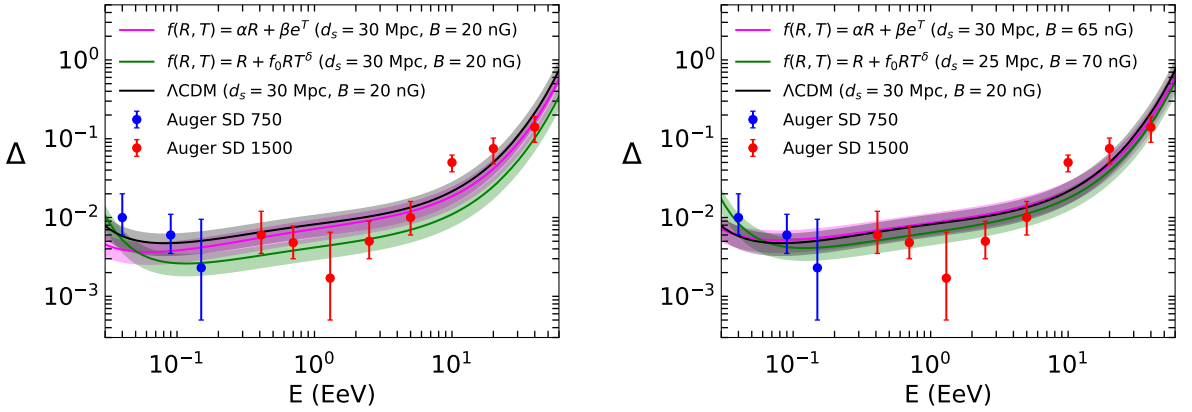


FIG. 5. Left: The unmodified anisotropy of the UHECRs as a function of energy E for the considered $f(R, T)$ models for $d_s = 30$ Mpc and $B = 20$ nG with the uncertainty colour bands. Right: The modified anisotropy of the UHECRs as a function of energy E for $d_s = 30$ Mpc, $B = 65$ nG and $d_s = 25$ Mpc, $B = 70$ nG for $f(R, T) = \alpha R + \beta e^T$ and $f(R, T) = R + f_0 R T^\delta$ respectively, with the uncertainty colour bands. The observational data are taken from the Auger [89].

We summarised the results of this study in Fig. 5, wherein the left panel represents the comparison between the predictions of the $f(R, T)$ models and the Λ CDM model, all calculated for $d_s = 30$ Mpc and $B = 20$ nG. Uncertainty bands are added to both $f(R, T)$ gravity models to account for potential variations in model parameters. The experimental data from Auger SD 750 and SD 1500 are well accommodated by the predictions, with the shaded regions indicating a reasonable overlap. The right panel of Fig. 5 showcases the results of the $f(R, T)$ models with optimized parameter sets ($d_s = 30$ Mpc, $B = 65$ nG for $f(R, T) = \alpha R + \beta e^T$, and $d_s = 25$ Mpc, $B = 70$ nG for $f(R, T) = R + f_0 R T^\delta$), along with the Λ CDM prediction for $d_s = 30$ Mpc, $B = 20$ nG. The adjustments in B and d_s for the $f(R, T)$ models further enhance their compatibility with the Auger datasets. The addition of uncertainty bands provides a robust representation of theoretical predictions and demonstrates the sensitivity of anisotropy to the theoretical parameters. The inclusion of uncertainty bands in the updated predictions emphasizes the sensitivity of anisotropy to the models' assumptions. These results underline the importance of precise tuning of $f(R, T)$ parameters, as changes in B and d_s significantly influence the alignment with data. Moreover, the ability of $f(R, T)$ gravity models to suppress anisotropy at intermediate energies compared to Λ CDM suggests that modified gravity effects could play a vital role in explaining CRs propagation and their interactions in extragalactic magnetic fields. Overall, our results indicate that the $f(R, T)$ gravity models can effectively reproduce the observed energy-dependent anisotropy of UHECRs incorporating the effects of magnetic fields and source separations.

ACKNOWLEDGEMENTS

UDG is thankful to the Inter-University Centre for Astronomy and Astrophysics (IUCAA), Pune, India for the Visiting Associateship of the institute.

-
- [1] P. Blasi, *Astron. Astrophys. Rev.* **21**, 70 (2013), [arXiv:1311.7346].
- [2] E. G. Berezhko, H. Volk, *Astrophys. J. Lett.* **661**, L175 (2007) [arXiv:0704.1715].
- [3] J. W. Hewitt, M. Lemoine-Goumard, *Comptes rendus Physique* **16**, 674 (2015).
- [4] D. Harari, S. Mollerach, E. Roulet, *Phys. Rev. D* **89**, 123001 (2014) [arXiv:1312.1366].
- [5] S. Mollerach, E. Roulet, *Phys. Rev. D* **105**, 063001 (2022) [arXiv:2111.00560v2].
- [6] P. Abreu et al. (Pierre Auger Collaboration), *Astrophys. J. Lett.* **762** (2013) L13 [arXiv:1212.3083v1].
- [7] R.U. Abbasi (Telescope Array Collaboration), *Astropart. Phys.* **86**, 21 (2017) [arXiv:1608.06306v2].
- [8] A. Aab et al. (Pierre Auger Collaboration), *Science* **357**, 1266 (2017) [arXiv:1709.07321v1].
- [9] A. Aab et al. (The Pierre Auger Collaboration), *Phys. Rev. Lett.* **125**, 121106 (2020) [arXiv:2008.06488].
- [10] A. Aab et al. (The Pierre Auger Collaboration), *Phys. Rev. D* **102**, 062005 (2020) [arXiv:2008.06486].
- [11] P. Abreu et al. (Pierre Auger Collaboration), *Eur. Phys. J. C* **81** (2021) 966 [arXiv:2109.13400v3].
- [12] V. Novotný, the Pierre Auger Collaboration, *PoS ICRC* **324** (2021).
- [13] A. M. Hillas, *Phys. Lett. A* **24**, 677 (1967).
- [14] G. R. Blumenthal, *Phys. Rev. D* **1**, 1596 (1970).
- [15] V. Berezhinsky, A. Z. Gazizov, S. I. Grigorieva, *Phys. Rev. D* **74**, 043005 (2006) [arXiv:hep-ph/0204357].
- [16] M. Lemoine, *Phys. Rev. D* **71**, 083007 (2005) [arXiv:astro-ph/0411173].
- [17] R. U. Abbasi et al. (HiRes Collaboration), *Phys. Rev. Lett.* **100** (2008) 101101 [arXiv:astro-ph/0703099v2].
- [18] J. Abraham et al. (The Pierre Auger Collaboration), *Phys. Rev. Lett.* **101**, 061101 (2008) [arXiv:0806.4302v1].
- [19] T. Abu-Zayyad et al. (Telescope Array Collaboration), *Astrophys. J.* **768**, L1 (2013).
- [20] K. Greisen, *Phys. Rev. Lett.* **16**, (1966) 748.
- [21] G.T. Zatsepin, V.A. Kuz'min, *JETP Lett.* **4**, 78 (1966).
- [22] J. Abraham et al., (Pierre Auger Collaboration), *Astropart. Phys.* **31**, 399 (2009) [arXiv:0903.1127v2].
- [23] T. Abu-Zayyad et al. (Telescope Array Collaboration), *Phys. Rev. D* **88**, 112005 (2013) [arXiv:1304.5614].
- [24] P. Abreu et al. (Pierre Auger Collaboration), *JCAP* **05**, 021 (2023) [arXiv:2209.05926].
- [25] P. Abreu et al., (Pierre Auger Collaboration), *Astrophys. J.* **755**, L4 (2012).
- [26] M. G. Aartsen et al., (IceCube Collaboration), *Phys. Rev. D* **89**, 062007 (2014) [arXiv:1311.7048].
- [27] A. Aab et al. (Pierre Auger Collaboration), *JCAP* **10**, 022 (2019) [arXiv:1906.07422].
- [28] P. Abreu et al., (Pierre Auger Collaboration), *Astrophys. J.* **760**, 148 (2012).
- [29] J. Abraham et al., (Pierre Auger Collaboration), *Phys. Rev. Lett.* **104**, 091101 (2010) [arXiv:1002.0699v1].
- [30] Pierre Auger Collaboration, *JCAP* **02**, 026 (2013).
- [31] A. Aab et al. (Pierre Auger Collaboration), *Phys. Rev. D* **90**, 122005 (2014) [arXiv:1409.4809].
- [32] A. Aab et al. (Pierre Auger Collaboration), *Phys. Rev. D* **90**, 122006 (2014) [arXiv:1409.5083].
- [33] A. Aab et al. (Pierre Auger Collaboration), *Phys. Rev. D* **96**, 122003 (2017).
- [34] S. Mollerach, E. Roulet, *Phys. Rev. D* **99**, 103010 (2019) [arXiv:1903.05722].
- [35] S. Mollerach, E. Roulet, *Prog. Part. Nucl. Phys.* **98**, 85 (2018) [arXiv:1710.11155].
- [36] O. Deligny, K. Kawata, P. Tinyakov, *PTEP* **2017**, 12A104 (2017) [arXiv:1702.07209].
- [37] O. Deligny, *Astropart. Phys.* **104**, 13 (2019) [arXiv:1808.03940].
- [38] A. Aab et al. (Pierre Auger Collaboration), *Astrophys. J.* **868**, 4 (2018) [arXiv:1808.03579].
- [39] P. Abeu et al., *Astrophys. J.* **935**, 170 (2022) [arXiv:2206.13492].
- [40] A. Aab. et al., (Pierre Auger Collaboration), *Astrophys. J. Lett.*, **853**:L29 (2018) [arXiv:1801.06160]
- [41] R. U. Abbasi et al.,(Telescope Array Collaboration), *Astrophys. J. Lett.* **898**, L28 (2020) [arXiv:2007.00023].
- [42] R. U. Abbasi et al.,(Telescope Array Collaboration), *Astrophys. J.* **862**, 91 (2018).
- [43] R. U. Abbasi et al.,(Telescope Array Collaboration), [arXiv:2110.14827].
- [44] P. Tinyakov et al., (Telescope Array Collaboration), *PoS ICRC*, **375** (2021)]
- [45] A. G. Reiss et al., *Astron. J.* **116**, 1009 (1998) [arXiv:astro-ph/9805201].
- [46] S. Perlmutter et al., *Astrophys. J.* **517**, 565 (1999) [arXiv:astro-ph/9812133].
- [47] D. N. Spergel et al., *Astrophys. J. Suppl. S* **170**, 377 (2007) [arXiv:astro-ph/0603449].
- [48] P. Brax, *Rep. Prog. Phys.* **81**, 1 (2018).
- [49] E. J. Copeland, M. Sami, S. Tsujikawa, *IJMP D* **15**, 1753-1936 (2006) [arXiv:hep-th/0603057].
- [50] U. D. Goswami, H. Nandan, M. Sami, *Phys. Rev. D* **82**, 103530 (2010).
- [51] S. Nojiri, S.D. Odintsov, V.K. Oikonomou, *Phys. Rep.* **692**, 1 (2017).
- [52] P. Sotiriou, V. Faraoni, *Rev. Mod. Phys.* **82**, 451 (2010) [arXiv:0805.1726].
- [53] A. De Felice, S. Tsujikawa, *Living Rev. Relativ.* **13**, 3 (2010)
- [54] D. J. Gogoi, U. D. Goswami, *IJMP D* **31**, 2250048 (2022) [arXiv:2108.01409].
- [55] U. D. Goswami, K. Deka, *IJMP D* **22**, 13 (2013) 1350083 [arXiv:1303.5868].

- [56] J. B. Jiménez et al., *Coincident General Relativity*, *Phys. Rev. D* **98**, 044048 (2018) [arXiv:1710.03116].
- [57] T. Harko et al., *Coupling matter in modified Q gravity*, *Phys. Rev. D* **98**, 084043 (2018) [arXiv:1806.10437].
- [58] S. Mandal, P. K. Sahoo, J. R. L. Santos, *Phys. Rev. D* **102**, 024057 (2020) [arXiv:2008.01563].
- [59] S. Mandal, D. Wang, P. K. Sahoo, *Phys. Rev. D* **102**, 124029 (2020) [arXiv:2011.00420].
- [60] N. Frusciante, *Phys. Rev. D* **103**, 044021 (2021) [arXiv:2101.09242].
- [61] P. Sarmah, A. De, U. D. Goswami, *Phys. Dark Universe* **40**, 101209 (2023) [arXiv:2303.05905].
- [62] S. Bahamonde, C. G. Böhmer, M. Wright, *Phys. Rev. D* **92**, 104042 (2015).
- [63] S. Bahamonde, C. G. Böhmer, M. Krššák, *Phys. Lett. B* **775**, 37 (2017).
- [64] T. Azizi, E. Yaraie, *Int. J. Mod. Phys. D* **23** (2014) 1450021.
- [65] O. Bertolami, P. Frazo, J. Pramos, *Phys. Rev. D* **83** (2011) 044010
- [66] S. Nesseris, *Phys. Rev. D* **79** (2009) 044015
- [67] T. Futamase, K.I. Maeda, *Phys. Rev. D* **39** (1989) 399
- [68] J.P. Uzan, *Phys. Rev. D* **59** (1999) 123510
- [69] T. Harko, F.S.N. Lobo, *Eur. Phys. J. C* **70** (2010) 373
- [70] T. Harko, F.S.N. Lobo, S. Nojiri, S.D. Odintsov, *Phys. Rev. D* **84** (2011) 024020.
- [71] M. Sharif, M. Zubair, *J. Cosmol. Astropart. Phys.* **03** (2012) 028.
- [72] F.G. Alvarenga et al., *Phys. Rev. D* **87** (2013) 103526.
- [73] R. Zaregonbadi, M. Farhoudi, N. Riazi, *Phys. Rev. D* **94** (2016) 084052
- [74] P. Rudra, *Eur. Phys. J. Plus* **130** (4) (2015) 66
- [75] M. Sharif, A. Siddiq, *Gen. Relativ. Gravit.* **51** (6) (2019) 74.
- [76] J. Bora, U. D. Goswami, *Phys. Dark Universe* **38**, 101132 (2022).
- [77] P. Mertsch, M. Ahlers, *JCAP* **11**, 048 (2019) [arXiv:1909.09052v2].
- [78] D. Harari, S. Mollerach, E. Roulet, *Phys. Rev. D* **103**, 023012 (2021) [arXiv:2010.10629v2].
- [79] M. Ahlers, P. Mertsch, *Prog. Part. Nucl. Phys.* **94**, 184 (2017) [arXiv:1612.01873v1].
- [80] S. Mollerach, E. Roulet, O. Taborda, *JCAP* **12**, 021 (2022) [arXiv:2207.11540v2].
- [81] A. U. Abeysekara et al., *Astrophys. J* **871**, 96 (2019).
- [82] M. Chakraborty et al., (Grapes-3 Collaboration), *PoS ICRC* **395** (2021).
- [83] N. Globus et al., *MNRAS* **484**, 4167 (2019).
- [84] G. Sigl, M. Lemoine, P. Biermann, *Astropart. Phys.* **10** (1999) 141
- [85] S. P. Sarmah, U. D. Goswami, *Eur. Phys. J. C* **84**, 419 (2024) [arXiv:2303.16678].
- [86] S. P. Sarmah, U. D. Goswami, *Astropart. Phys.* **163**, 103005 (2024) [arXiv:2309.14361].
- [87] S. P. Sarmah, U. D. Goswami, [arXiv:2411.00366].
- [88] S. P. Sarmah, U. D. Goswami, [arXiv:2406.11902].
- [89] A. Aab et al., (Pierre Auger Collaboration), *Astrophys. J.* **891**, 142 (2020) [arXiv:2002.06172].
- [90] J. L. Han, *Annu. Rev. Astron.* **255**, 111 (2017).
- [91] Y. Hu et al., *Astrophys. J.* **941**, 133 (2022).
- [92] U. Chadayammuri, *MNRAS* **512**, 2 (2022).
- [93] L. Feretti et al., *Astron. Astrophys. Rev.* **20**, 54 (2012).
- [94] J. P. Vallée, *New Astro. Rev.* **55**, 91 (2011).
- [95] F. Vazza et al., *Class. Quantum Grav.* **34**, 234001 (2017).
- [96] G. Sigl, F. Miniati and T. A. Ensslin, *Phys. Rev. D* **70**, 043007 (2004) [arXiv:astro-ph/0401084]
- [97] V. Berezhinsky, A. Z. Gazizov, *Astrophys. J.* **643**, 8 (2006) [arXiv:astro-ph/0512090].
- [98] S. I. Syrovatskii, *Soviet Astro.* **3**, 22 (1959).
- [99] P. Rudra, K. giri, *Nucl. Phys. B* **967**, 115428 (2021)
- [100] N. Aghanim et al., (Planck Collaboration), *A & A* **641**, A6 (2020) [arXiv:1807.06209].
- [101] K. Nakamura and Particle Data Group, *J. Phys. G: Nucl. Part. Phys.* **37**, 075021(2010).
- [102] R. Solanki et al., *Phys. Dark Universe*, **32**, 100820 (2021), [arXiv:2105.00876].
- [103] J. M. González, S. Mollerach, E. Roulet, *Phys. Rev. D* **104**, 063005 (2021) [arXiv:2105.08138].
- [104] S. Mollerach, E. Roulet, *JCAP* **10** 013 (2013) [arXiv:1305.6519v1].
- [105] A. D. Supanitsky, *JCAP* **04**, 046 (2021) [arXiv:2007.09063v2].